A POTENTIAL FUNCTION DERIVATION OF A CONSTITUTIVE EQUATION FOR INELASTIC MATERIAL RESPONSE[*]

Donald C. Stouffer and Nader Abu El Foutouh
University of Cincinnati
Cincinnati, Ohio 45221

ABSTRACT

Physical and thermodynamic concepts are used to develop a potential function for application to high temperature polycrystalline material response. Inherent in the formulation is a differential relationship between the potential function and constitutive equation in terms of the state variables. Integration of the differential relationship produces a state variable evolution equation that requires specification of the initial value of the state variable and its time derivative. Analysis of these conditions showed that the initial loading rate, which is directly related to the initial hardening rate, can significantly influence subsequent material response. This effect is consistent with observed material behavior on the macroscopic and microscopic levels, and may explain the wide scatter in response often found in creep testing. The material used for the study, cast and wrought IN100 at $732^{o}C$, was tested in tension at different strain rates, creep, stress relaxation, and reversed inelastic flow.

INTRODUCTION

The research presented in this paper is directed toward developing a state variable constitutive model for metals in high temperature environment where rate effects are important. The underlying concept used in the model is to develop a consistent system of equations to predict the inelastic strain rate and evolution of the state variables that are derivable from a potential function. The essential structure of the theory is based on the maximum plastic work inequality, the rate of work hardening inequality, and dislocation dynamics.

The maximum plastic work inequality, expressed using the concept of a yield surface, can be written as (refs. 1 and 2)

$$(\sigma_{ij} - \sigma_{ij}^{o})d\epsilon_{ij}^{I} \geq 0. \qquad (1.1)$$

The quantity $d\epsilon_{ij}^{I}$ is the inelastic strain increment due to the stress step $\sigma_{ij} - \sigma_{ij}^{o}$. The stress σ_{ij} is on the current yield surface and σ_{ij}^{o} is any other stress either inside or on the yield surface. The inequality requires that the inelastic strain increment is normal to the yield surface and that all yield surfaces are convex. Eq. (1.1) is an axiom resulting from observed plastic behavior of metals. It is not derivable from thermodynamics and is not necessarily valid for all materials. It does, however, capture the essence of how many metals behave.

The property of work hardening, as identified with a large class of metals, can be further characterized. In these materials it has been consistently observed that the stored energy of cold work, W^h, increases with deformation at a decreasing rate during a continuous deformation history. This can be expressed by

$$dW_2^h - dW_1^h \leq 0 , \qquad\qquad (1.2)$$

where dW_1^h and dW_2^h are the increments of stored energy associated with identical strain (or stress) increments in two different stored worked states W_1^h and W_2^h such that $W_2^h > W_1^h$ (ref. 3). The exact structure of a cold worked state is not fully understood, however, it is generally·accepted that the energy is stored through the development of a system of dislocations (ref. 4 and 5).

In the initial state of deformation dislocations multiply and tend to arrange themselves into groups or clusters occupying only a small fraction of the material volume. Most of the deformed material is dislocation free. As deformation increases the dislocation clusters form continuous walls separating relatively perfect cells. With further strain, secondary slip systems are activated and the density of dislocations increases with other point defects appearing. The cell size decreases at a decreasing rate as strain increases and tends to stabilize. The cell size and dislocation density at any time are influenced by the initial microstructure, temperature and loading history up to that time. In addition, it is important to recognize that a substantial portion of the character of the microstructure is established early in the load history when the observed macroscopic inelastic strain is very small.

In some cases, the stored energy is partially recovered in time at elevated temperature or fully recovered through recrystalization. This effect could be important for metals at high· temperature that have been work hardened in the initial configuration. This situation is typical of cast and wrought super-alloys. In the case of recovery, $W_2^h < W_1^h$, and the stored energy increments dW_1^h

154

and dW_2^h are both negative. In this case, eq. (1.2) requires the rate of change of recovery to be positive. That is, softening occurs at an increasing rate; conversely, hardening occurs at a decreasing rate, and both hardening and softening tend to stabilize.

The maximum plastic work inequality and the rate of work hardening inequality satisfy most observed response in metals at high temperature under continuous load histories. However, the essence of the theory can be easily extended by a broader class of materials and load histories by requiring the two inequalities hold together rather than individually; that is

$$(\sigma_{ij} - \sigma_{ij}^o)d\varepsilon_{ij}^I - (dW_2^h - dW_1^h) \geq 0 \ . \tag{1.3}$$

A similar relation was suggested by Ponter (refs. 5 and 6) and the consequences are extensive. First, since the stored energy is generally small compared to the total plastic work during a typical deformation history, the restriction on the hardening or softening rate (eq. (1.2)) can be softened in some cases. This allows, for example, a jump in the rate plastic working to produce a jump in the rate of work hardening that is not restricted by eq. (1.2). The effect appears possible in situations where there are jumps in strain rate early in the development of microstructure.

Another essential feature of the constitutive model is to use the result of Rice (ref. 7) showing that the components of an inelastic strain rate tensor, $\dot{\varepsilon}_{ij}^I$, are derivable, at each instant during the deformation history, from a potential function, Ω, of the stress, i.e.

$$\dot{\varepsilon}_{ij}^I = \frac{\partial \Omega[\underline{\sigma}, \text{history}]}{\partial \sigma_{ij}} \ . \tag{1.4}$$

This result is based on the physical notion of conventional crystalline deformation: At a given slipped state, the rate of permanent shearing on a particular slip system depends on the stress at that point only through the shear stress acting on the slip system. Thus, for a given prior history, eq. (1.4) was shown to give time dependent stress strain equations consistent with both plausible macroscopic and microscopic idealizations. More recently, Ponter and Leckie (ref. 8) extended the formulation to polycrystalline metals at high temperature. Following the methods in ref. 6 they established a potential function for a constitutive equation of the Baily (ref. 9) and Orowan (ref. 10) type that contains one state variable, s, to describe the hardness or stored

energy of the material. In the Ponter-Leckie development the assumption of a local (microscopic) potential was essential to establish a macroscopic potential that can be used to derive both the inelastic flow equation and state variable evolution equation. The Baily-Orowan the macroscopic flow equation contains an over stress argument of the type $\phi - s$, where ϕ is a scalar function of the stress tensor.

Another state variable constitutive equation that uses a single state variable to describe the hardness or resistance to inelastic flow was developed by Bodner and Partom (refs. 11 and 12). Inherent in the representation is the absence of a yield surface. That is, the inelastic strain rate is non-zero for all non-zero values of stress. This is a continuous flow equation without separate loading and unloading conditions. It has been used to successfully predict the response of two superalloys at high temperature (refs. 13 and 14). In part, the success may result from using the entire load history rather than excluding the load history inside the yield surface. For example, recall that the character of the dislocation substructure is established very early in the deformation history prior to classical yield.

Another key feature of the Bodner-Partom model is that the specific form of the flow equation was motivated by dislocation dynamics. Both of the well accepted representations for dislocation velocity, developed by Gilman (ref. 15) and Vreeland (ref. 16) are embodied in the Bodner-Partom formulation. One shortcoming of the Bodner-Partom representation is that the basic structure of the evolution equation for the hardness state variable is developed by phenomenological methods. The evolution equation is consistent with the observed properties of stored energy (eq. (1.2)) but does not possess a formal mathematical or physical derivation.

Specifically, in this paper it is shown that the concept of a macroscopic inelastic potential function is compatible with the essential features of high temperature material response expressed in eq. (1.3) . A potential function concept is then used to derive a state variable evolution equation directly from the inelastic flow equation. A specific example is developed using the Bodner-Partom representation. It is shown that the Bodner-Partom evolution equation has a mathematical structure very similar to the derived evolution equation. However, the derived evolution equation has a new important property. The derived representation depends on the initial hardening rate that can vary from test to test for the same initial material microstructure. The representation

156

is used to predict the response of IN100 at $732^{O}C$. The material constants are determined from tensile response data and the experimental response in, creep, stress relaxation and reversed inelastic flow is analyzed.

II DEVELOPMENT OF A POTENTIAL FUNCTION FORMULATION

Let us introduce a state variable Z as a macroscopic measure of the effect of the dislocation microstructure on deformation. It is designated as the hardness or resistance to inelastic flow and the units are that of stress. Similarly a macroscopic strain state variable, ε^h, is defined as a measure change in geometry associated with the development of dislocation microstructure.

The variables Z and ε^h are scalar functions of tensor valued arguments and defined so that an increment of stored energy of cold work can be calculated as

$$dW^h = Zd\varepsilon^h = d\dot{\varepsilon}^h dt \qquad (2.1)$$

It is required that the stored energy increment, dW^h, and hence the valuables Z and ε^h, satisfy the conditions outlined in the Introduction. The increment of inelastic work associated with an increment of inelastic deformation is

$$dW^I = \sigma_{ij}d\varepsilon_{ij}^I = \sigma_{ij}\dot{\varepsilon}_{ij}^I dt \qquad (2.2)$$

In a constant hardness state the maximum plastic work inequality (eq. (1.1)) can be written as

$$\dot{\varepsilon}_{ij}^I d\sigma_{ij} \geq 0, \quad Z = \text{const.} \qquad (2.3)$$

Similarly, the rate of work hardening inequality, for constant stress eq. (1.2) can be rewritten as

$$\dot{\varepsilon}^h dZ \leq 0, \qquad \sigma_{ij} = \text{const.} \qquad (2.4)$$

and the combined inequality (eq. (1.3)) is

$$\dot{\varepsilon}_{ij} \left| \begin{matrix} d\sigma_{ij} \\ Z = \text{const.} \end{matrix} \right. - \dot{\varepsilon}^h \left| \begin{matrix} dZ \geq 0. \\ \sigma_{ij} = \text{const.} \end{matrix} \right. \qquad (2.5)$$

Using the result of Rice (eq. (1.4)) there exists a potential function $\phi(\underset{\sim}{\sigma},Z)$ such that

$$\dot{\varepsilon}_{ij}^I = \frac{\partial\phi(\underset{\sim}{\sigma}, Z)}{\partial\sigma_{ij}} \qquad . \qquad (2.6)$$

Further, using the eqs. (2.5) and (2.6), and the result of Ponter (ref. 17), let us assume that for ϕ to exist and be physically acceptable, that

$$\dot{\varepsilon}^h = - \frac{\partial\phi[\sigma, Z]}{\partial Z} \qquad (2.7)$$

and

$$\frac{\partial\phi}{\partial\sigma_{ij}} d\sigma_{ij} + \frac{\partial\phi}{\partial Z} dZ = d\phi \geq 0.$$

Therefore, ϕ exists and it is convex in the space $\{\sigma, Z\}$ (ref. 16). The existence of the potential function $\phi(\sigma, Z)$ is consistent with the essential structure of work hardening or softening metal plasticity. As a result of the existance of ϕ and from eqs. (2.6) and (2.7) it follows that

$$\frac{\partial\dot{\varepsilon}^h}{\partial\sigma_{ij}} = - \frac{\partial\dot{\varepsilon}^I_{ij}}{\partial Z} \quad . \qquad (2.8)$$

Using the idea of an instantaneous tangent modulus in one dimensional plasticity, the stress rate state variable $\dot{Z}$ can be related to the strain rate variable $\dot{\varepsilon}^h$ by the function h; i.e.

$$\dot{Z} = h\dot{\varepsilon}^h = -h \frac{\partial\phi}{\partial Z} \quad . \qquad (2.9)$$

That is, h is the instantaneous slope of the $\dot{Z} \sim \dot{\varepsilon}^h$ response curve. For the following analysis let $h = h(Z,...)$ be independent of the current stress.

Finally, eq. (2.8) can be used to derive the state variable evolution equation directly from the flow equation. Let us assume $\dot{\varepsilon}^I_{ij} = \dot{\varepsilon}^I_{ij}(\sigma, Z)$ is specified, then from eq. (2.8) and (2.9)

$$d\dot{Z} = - h \frac{\partial\dot{\varepsilon}^I_{ij}}{\partial Z} d\sigma_{ij} + df(Z,...) \qquad (2.10)$$

where f is independent of stress. Integrating on the time interval [0,t], the evolution equation for the hardness can be written as

$$\dot{Z}(t) - \dot{Z}_0 = -h \int_{\sigma_{ij}(0)}^{\sigma_{ij}(t)} \frac{\partial\dot{\varepsilon}^I_{ij}}{\partial Z} d\sigma_{ij} + [f(Z,...) - f(Z_0,...)] \quad . \qquad (2.11)$$

The integral can be evaluated for any specific choice flow law involving only one state variable.

Embodied in eq. (2.11) is an important property that is not widely recognized. The parameters $\dot{Z}_0 = \dot{Z}(0)$ and $Z_0 = Z(0)$ are initial conditions. The parameter Z_0 describes the initial state of the microstructure that, for example, would be the same for all specimens from the same heat of material. However, $\dot{Z}_0$ is the initial rate of hardening of the microstrucutre and would be expected to vary from test to test, depending on the initial loading conditions.

III Bodner-Partom Constitution Equations

The Bodner-Partom constitutive equation (refs. 11, 12, 18) is a fully developed three dimensional theory that has even been extended to anisotropic materials (refs. 19 and 20). Since the main purpose of the paper is to evaluate the properties of the evolution equation, it is convenient to restrict the analysis to a one dimensional form of the constitutive equation. This is consistent with the accompanying experimental program.

The isotropic constitutive theory of Bodner and Partom is based on the assumption that the total strain rate, $\dot{\varepsilon}(t)$, can be separated into elastic, $\dot{\varepsilon}^e(t)$, and inelastic, $\dot{\varepsilon}^I(t)$, components. Let E represent the elastic modulus, then the Bodner-Partom equation can be written in a one dimensional form as

$$\dot{\varepsilon}(t) = \frac{\dot{\sigma}(t)}{E} + \dot{\varepsilon}^I(t) \tag{3.1}$$

where $\sigma(t)$ is the current value of the stress. Inherent to the theory is that the inelastic strain rate is non-zero for all non-zero values of stress. The specific representation used by Bodner and his co-workers for the inelastic strain rate is given by

$$\dot{\varepsilon}^I(t) = D_0 \frac{\sigma(t)}{|\sigma(t)|} \exp\left[-\frac{(n+1)}{2n}\left(\frac{Z^2}{\sigma^2}\right)^n\right] . \tag{3.2}$$

The constant D_0 represents a limiting value of the inelastic strain rate and is generally taken at $2\times10^4/\sqrt{3}$ sec^{-1} unless the strain rates are very high. The constant n controls the strain rate sensitivity and $Z(t)$ is the hardness state variable. The general mathematical structure of eq. (3.2) is based on dislocation dynamics expressed in the context of continuum mechanics and has proven consistent with the observed response for many metals. The formulation is similar to the classical yield surface theory. The structure of the Prandtl-Reuss formulation is preserved, but a yield surface itself is not part of eqs. (3.1) and (3.2).

Necessary for the use of the above equations is a representation for the state variable Z. The specific representation proposed by Bodner et. al. (ref. 18) and used for superalloys (refs. 13, 14 and 21) is based on the concept that only the inelastic rate of working $\dot{W}^I$ and the current hardness control the rate of hardening. The representation is written as

$$\dot{Z} = m(Z_1 - Z)\dot{W}^P - AZ_1 \left(\frac{Z-Z_2}{Z_1}\right)^r \tag{3.3}$$

with Z_0 designated as the inital value of Z. The two terms in eq. (3.3) are defined so that $AZ_1[(Z-Z_2)/Z_1]^r$ is negligible during rapid load histories. Thus, during a tensile test that is fast compared to creep test, eq. (3.3) reduces to the first term alone. The constant Z_1 corresponds to the maximum value for Z and m is an exponential coefficient controlling the rate of hardening. For a long time response, such as creep, a second term corresponding to hardening recovery is necessary. During the minimum creep rate both $\dot{\epsilon}^P$ and σ are constant, thus Z is constant $(\dot{Z} = 0)$ and the rate of hardening must equal the rate of recovery. The coefficient Z_2 corresponds to the minimum recoverable value of hardness, and A and r are the coefficient and exponent, respectively, controlling the rate of hardening recovery.

At this point in the paper it is now possible to carry out one specific objective: Derive an evolution equation for $\dot{Z}$ by using eq. (3.2) in eq. (2.11) and to compare the result to eq. (3.3). To begin, let us define

$$B = D_0 \left(\frac{n+1}{2n}\right)^{1/2n} \text{ and } R = \frac{n+1}{2n}\left(\frac{Z}{\sigma}\right)^{2n} \tag{3.4}$$

so that the integral in eq. (2.11) can be written as

$$I = B \int R^{-1/2n} e^{-R} dR . \tag{3.5}$$

For continuous histories eq. (3.5) can be integrated by parts N times to obtain a series representation. Letting $p = 1/2n$, the series can be written as

$$I(R) = B e^{-R}R^{-p}\left[\frac{R}{(1-p)} + \frac{R^2}{(1-p)(2-p)} + \frac{R^3}{(1-p)(2-p)(3-p)} + \dots\right] \tag{3.6}$$

which converges for all R on $(0,\infty)$. The function I(R) is almost constant for large values of R (small values of stress) and decays with decreasing R (increasing stress). In this application of eq. (3.6) the constants D_0 and n are generally known so eq. (3.6) is totally defined.

Finally, since eq. (3.5) could be integrated to obtain eq. (3.6), then eq. (3.6) is an exact differential. This implies that the contribution of

160

I(R) to the current hardening rate depends only on the current value of the state, Z, and the current stress. Thus, for all histories producing the same state and stress the integral term will have the same contribution to the hardening rate.

IV PROPERTIES OF THE TWO EVOLUTION EQUATIONS

The derived evolution Equations, (eqs. (2.11) and (3.6)), can be put in a form similar to the Bodner-Partom eq. (3.3). Noting from eqs. (3.2) and (3.4) that I(R) can be written as

$$I(R) = g(\frac{\sigma}{Z})\dot{\varepsilon}^I \tag{4.1}$$

where

$$g(\frac{\sigma}{Z}) = D_0(\frac{n+1}{2n})^{1/2n} R^{-p}[\frac{R}{(1-p)} + \frac{R^2}{(1-p)(2-p)} + \frac{R^3}{(1-p)(2-p)(3-p)} + ...] \tag{4.2}$$

and $R(\frac{Z}{\sigma})$ is given by eq. (3.4). Thus, the derived evolution Equation, (eq. (2.11)), becomes

$$\dot{Z} = \dot{Z}_0 - h[g(\frac{Z}{\sigma}) - g_0(\frac{Z}{\sigma})]\dot{\varepsilon}^I + [f(Z,...) - f(Z_0,...)]. \tag{4.3}$$

The Bodner-Partom Evolution Equation (eq. (3.3)) can be rewritten for convenience as

$$\dot{Z} = m(Z_1 - Z)\sigma\dot{\varepsilon}^I - AZ_1(\frac{Z-Z_2}{Z_1})^r . \tag{4.4}$$

Direct comparison of eqs. (4.3) and (4.4) shows a very strong mathematic similarity. Both equations have two terms of similar type. One term is linear in the inelastic strain rate, $\dot{\varepsilon}^I$, and the other term is independent of the stress σ. The derived evolution equation has the initial hardening rate term $\dot{Z}_0$. The coefficient of the strain rate term in the derived equation is a product of a modulus h and a non-linear function of $(\frac{Z}{\sigma})$; whereas, the corresponding term in the Bodner-Partom is linear in both σ and Z. The function $f(Z,...)$ in the derived equation is consistent with logarithmic function of Z in the Bodner-Partom equation. In general, eq. (4.4) can be considered almost a special case of eq. (4.3).

To evaluate the properties of the derived evolution equation further it is convenient to develop a representation for the function $f(Z,...)$. A power series expansion of f in Z would produce a series of exponential time terms when

161

eq. (4.3) is solved. Since the general solution is exponential in nature, a reasonable approximation is to use a single exponential term. Thus, let us assume a linear representation, namely

$$f(Z) - f(Z_0) = -\alpha(Z - Z_0) \tag{4.5}$$

where α is a parameter that is independent of Z and σ. Further, in order for the representation for Z to approach a stable asymptotic value it is necessary for $\alpha > 0$. It is expected that this representation should contain many of the essential features.

Even though the mathematical structure of eqs. (4.3) and (4.4) is similar, the physical interpretation of the terms is different. First notice that $t = 0$, $\dot{Z} = 0$ in eq. (4.4) whereas $\dot{Z} = \dot{Z}_0$ in eq. (4.3). It is expected that the initial hardening rate should depend on the initial loading conditions, that is $\dot{Z}_0 = \dot{Z}_0(\dot{\varepsilon}_0) = \dot{Z}_0(\dot{\sigma}_0/E)$ where $\dot{\varepsilon}_0$ and $\dot{\sigma}_0$ are the initial strain and stress rates. This adds considerable flexability to the model and is consistent with the initial formation of dislocation microstructure as described earlier. Next, the strain rate term in the third term of eq. (4.3) produce basic tensile response properties and the stable value for Z. The strain rate term of eq. (4.3) and the second term of eq. (4.4) characterize the long time recovery response properties of the model.

<div align="center">V EXPERIMENTAL PROGRAM</div>

Sixteen mechanical tests have been conducted on IN100 at 732°C (1350°F) at the Air Force Wright Aeronautical Laboratory, Ohio and Mar-Test Inc., Cincinnati, Ohio. The material was obtained at different times from different heats resulting in five groups of specimens designated as series C, G, T, GT and ENTEN. The experimental program, summarized in Table 1, includes eight tensile tests, seven creep tests and one combined test. The controlled experimental variable is shown in Table 1 and the observed stable values for stress or secondary creep rate is also given for the tensile and creep tests, respectively.

The results of seven tests conducted under constant strain rate control ranging from 1.4×10^{-3} sec^{-1} to 1.6×10^{-6} sec^{-1} and one test under constant head rate control at 8.3×10^{-4} sec^{-1} are shown in fig. 2. There is significant variation in the level of the stress response due to the imposed variation in strain and head rate. Note, however, the total accumulated strain in these tests is not important since several of the specimens were not failed. For four

different values of strain rate (Tests 2, 4, 6 and 8) the response obtained a maximum stress and maintained that value of stress for all subsequent values of strain. However for Tests 5, 7 and 9 a different response was obtained. In these experiments the value of the stress decayed from the maximum value obtained at about one percent strain. In test 5 the amount of reduction in stress to a lower stable value was small. In Test 7, at a lower strain rate, the reduction in stress to a stable value was larger; and in Test 9, the stress did not stabilize at a lower level. This wide variation in response might arise since the eight specimens are from four different heats. Since both types of response were observed at both AFWAL and Mar-Test Inc., it cannot be accepted as an experimental problem.

The results of six creep tests are shown collectively in fig. 6b for up to 100 minutes. The variation in the creep stress was almost twofold 496 to 896 MPa (72 to 130 KSI), and the corresponding minimum creep rates are given in Table 1. Although not shown, Test 10, 14 and 15 obtained tertiary creep at times ranging from 100 minutes to about 1200 minutes. The response curves do not exhibit a significant primary creep phase and most of the response is dominated by tertiary creep. This is typical of other superalloys. Test 20, creep at 896 MPa (130 KSI) shown in fig. 6b, is not ordered with respect to the other tests; however, this could result from speciments variation or loading conditions as discussed later.

If the deformation mechanism controlling the tensile tests and creep tests are the same, then the controlled and observed variables from the two types of tests shown in Table 1 correspond to the same deformation process. That is, the stable value of stress obtained in a strain rate controlled tensile tests should correspond to the creep stress with the same constant (secondary) creep rate as the tensile test. A plot of the observed and controlled variables for both the creep at tensile tests is given in fig. 1. Considering the data is over five decades of strain rate, there appears to be reasonable consistency between both types of tests. Tensile Tests 7 and 8 correspond very closely to creep Tests 19 and 18, respectively, as shown in fig. 1 and table 1. Thus, it does appear that the same basic deformation mechanisms control both creep and tensile behavior between 482 and 1100 MPa (70 and 164 KSI) at $732^{\circ}C$ ($1350^{\circ}F$).

163

The next step in predicting the response of IN100 at $732^\circ C$ is to determine the remaining material parameters in the evolution equation. This exercise is divided into two steps. First, constant strain rate histories are analyzed and then the results are extended to piecewise constant strain rate histories.

Constant strain rate histories. The evolution equation that is derived from the potential function can be written as

$$\dot{Z} = \dot{Z}_0 - \alpha(Z-Z_0) + h[I(0)-I(t)] \tag{6.1}$$

for continous deformation histories using eqs. (4.5) and (4.1) in eq. (4.2). During each constant strain rate tensile test the last term approaches a step to the steady value, Δ_{ss}. An approximation of the behavior can be made by replacing the integral term in eq. (6.1) by a step function. Thus, assume eq. (6.1) can be approximated by

$$\dot{Z} \cong \dot{Z}_0 - \alpha(Z-Z_0) + \Delta_{ss}\mu[t-t_n] \tag{6.2}$$

where t_n is the time of the unit step $\mu[t-t_n]$. The solution of eq. (6.2) for the hardness variable yields

$$Z = Z_0 e^{-\alpha t} + (\frac{\dot{Z}_0+\alpha Z_0}{\alpha})(1-e^{-\alpha t}) + \frac{\Delta_{ss}}{\alpha} \mu[t-t_n](1-e^{-\alpha(t-t_n)}) \tag{6.3}$$

which is expected to be a reasonable approximation for times up to t_n and at times much larger than t_n.

Since a significant change in response occurs early in the history, let us define t_n as the time to reach the ultimate stress under a hypothetical elastic loading conditions using the initial strain rate; ie,

$$t_n = \frac{\sigma_\mu}{E\dot{\varepsilon}_0} \tag{6.4}$$

where σ_μ and $\dot{\varepsilon}_0$ are the ultimate stress and constant strain rate during each tensile test. The elastic modulus is denoted by E. Thus, the response up to time t_n characterizes the development of the microstructure before the onset of significant macroscopic inelastic deformation. The value of hardness, Z_n, expressed from eq. (6.3) as

$$Z_n = Z_0 + \frac{\dot{Z}_0}{\alpha} (1-e^{-\alpha t_n}) \tag{6.5}$$

and the steady state value (Long time) value is

$$Z_{ss} = \frac{\dot{Z}_0 + \alpha Z_0 + \Delta_{ss}}{\alpha} \quad . \tag{6.6}$$

Equations (6.5) and (6.6) can be used to evaluate the parameters in the evolution equation at three points: the initial condition Z_0 and $\dot{Z}_0$; the onset of significant inelastic flow, Z_n; and in the fully saturated condition, Z_{ss}.

The values of Z_n and Z_{ss} can be calculated directly from the tensile data for each test. Inverting eq. (3.2) and evaluating at time t_n gives

$$Z_n = \sigma_\mu [\frac{-2n}{n+1} \ell n(\frac{\dot{\varepsilon}_0}{D_0})]^{1/2n} \quad , \tag{6.7}$$

likewise at saturation

$$Z_{ss} = \sigma_{ss} [\frac{-2n}{n+1} \ell n(\frac{\dot{\varepsilon}_0}{D_0})]^{1/2n} \quad . \tag{6.8}$$

Comparing eq. (6.1) to eq. (6.2) and using eq. (6.8) yields

$$\Delta_{ss} = h[I(0) - I(\frac{Z_{ss}}{\sigma_{ss}})] \tag{6.9}$$

which can be used with eq. (6.6) to define the parameter h as

$$h = \frac{\alpha(Z_{ss}-Z_0)-\dot{Z}_0}{[I(0)-I(\frac{Z_{ss}}{\sigma_{ss}})]} \quad . \tag{6.10}$$

The parameter h, as, expected, is a function of history noting from eq. (6.8) that (Z_{ss}/σ_{ss}) is dependent only on the imposed constant strain rate $\dot{\varepsilon}_0$. The initial hardening rate can also be determined from eq. (6.5)

$$\dot{Z}_0 = \frac{\alpha(Z_n-Z_0)}{1-e^{-\alpha t_n}} \tag{6.11}$$

noting that Z_n can be determined from eq. (6.7).

The time parameter α can by estimated from the time required to obtain the steady state response. Assuming $e^{-\alpha t}$ vanishes at $\alpha t = 5$ and using saturation strain ε_∞, then $\alpha \varepsilon_\infty / |\dot{\varepsilon}_0| = 5$. In this example

$$\alpha = C_0 |\dot{\varepsilon}_0| \quad , \tag{6.12}$$

where $C_0 = 10$ $\sec^{-1}$ and the time response is also dependent upon the applied strain rate. The remaining parameter Z_0 is choosen by interactive computation to obtain the best fit for the lowest strain rate response curve. The permits including the recovery effect as well as strain hardening. This, analysis produced $\alpha_0 = 3275$MPa(475 KSI). The representations derived directly from the tensile data for use with eq. (6.7) and (6.8) are

$$\sigma_\mu = 6.8948(218.79 \ x^{-0.77934} - 58.65 \ x^{-2.9144})$$

and

$$\sigma_{ss} = 6.8948(162.048 \ x^{-0.31697} - 0.047656 \ x^{9.6381}) \qquad (6.13)$$

where $x = \log \dot{\varepsilon}/\log D_0$ and stress is in MPa(KSI). The representations were established to account for two different deformation mechanisms above and below approximately 900 MPa (see fig. 6). The other constants for IN100 used in the study were taken from ref. 14. They are

$$E = 1.50 \times 10^5 \text{ MPa}, \quad n = 0.70 \text{ and } D_0 = 2 \times 10^4/\sqrt{3} \ \sec^{-1}.$$

Piecewise Constant Histories. The representation for constant strain rate histories can be summarized by substituting eq. 6.10 into eq. 6.2 and identifying Z_{ss}/σ_{ss} from eq. (6.8) as a function of the applied strain rate, $\dot{\varepsilon}_0$, to get

$$\dot{Z} = \dot{Z}_0 - \alpha(Z-Z_0) + [\alpha(Z_{ss}-Z_0)-\dot{Z}_0] \ \frac{[I(0)-I(\frac{Z}{\sigma})]}{[I(0)-I(\dot{\varepsilon}_0)]} \ . \qquad (6.14)$$

Let us consider a step change in strain rate from $\dot{\varepsilon}_0$ to $\dot{\varepsilon}_1$ at time t_1. From eq. (3.1) it is seen that this produces a jump in the stress rate,

$$\Delta\dot{\sigma}_1 = E[(\dot{\varepsilon}_1-\dot{\varepsilon}_0)-(\dot{\varepsilon}_1^I-\dot{\varepsilon}_0^I)] \qquad (6.15)$$

but not a jump in the stress. Further it is expected that the inelastic strain rate would remain the same; therefore, from eq. (3.2), the value of the hardness Z is the same immediately before and after the jump in the strain rate. This implies that the microstructure does not change instantaneously. Note that eq. (6.15) also shows that separate unloading conditions are not required. If $\dot{\varepsilon}_1 = -\dot{\varepsilon}_0$, then $\Delta\dot{\sigma}_1 = -2E\dot{\varepsilon}_0$, which is very large compared to a stress rate near zero before the jump if the material is in the plastic range. Also, note that since the one test with reverse plastic flow does not indicate a significant amount of Bauschinger Effect, it is reasonable to assume an "isotropic hardening

rule" and use the same hardening rate equation for loading in both tension and compression.

It is expected, however, that a jump in strain rate would produce a jump in the hardening rate, $\dot{Z}$. From eq. (6.14), a jump in the value of $\dot{\varepsilon}_0$ to $\dot{\varepsilon}_1$ should produce a jump in $I(\dot{\varepsilon}_0)$, Z_{ss} and α. It is necessary to update $I(\dot{\varepsilon}_0)$ to $I(\dot{\varepsilon}_1)$ to maintain the asympotic value for Z. In this case, as time becomes large, $\dot{Z}$ approaches zero for any choice of Z_{ss} and α. Thus, Z_{ss} and α define the new microstructure corresponding new strain rate and time required to arrive at the new structure. For IN100,it was found that updating Z_{ss}, especially after several strain rate steps, produces erroneous results and estimating Z_{ss} from the initial strain rate produced much better results. Thus, due to the lack of more specific information, Z_{ss} was determined from the initial value of strain rate. This implies that the microstructure generated during the initial load secquence establishes some of the major features of the microstructure for all subsequent deformations. This appears to be reasonable for the simple deformation histories used in current study; but, may not be valid for all materials and all deformations. Finally, from the lack of better data during creep and stress relaxation testing, as fully explained later, it was decided to use the same value for α the entire history as a first approximation. Thus, for step changes in strain rate, the hardening rate described in eq. (6.14) is used with the values of α and Z_{ss} determined by the initial strain rate.

Extension to continuously varying strain rate histories could perhaps be modelled by using the current value for strain rate as described above. However, in the current paper only piecewise constant strain rate histories were used in the experimental program so it is difficult to test this hypothesis. Extension to other histories and materials requires additional development along with a better experimental description of microstructural changes.

VII CALCULATED AND PREDICTED RESULTS

The observed and calculated tensile response curves are shown in fig. 2. The calculated curves match the observed response with remarkable detail. The constants were determined with only two parameters, Z_0 and C_0, being determined by computational techniques. This was done using Curve 9 only. Further only

167

tensile data was used to determine the constants in eq. (6.13). All other predictions were made using only these constants.

It is interesting to note that the shape of both the observed and calculated response curves are not uniform. Curves 5, 6, 7 and 9 show elements of softening and hardening effects. Notice that there is the same ordering of the softening in curves 7 and 9, with almost no softening in curve 8. The value of $G = [I(0)-I(Z/\sigma)]/[I(0)-I(\dot{\epsilon}_U)]$ in eq. (6.14) for the tensile curves is shown in fig. 3. The effect of this term becomes important at about the yield strain. Thus, it is responsible for describing the majority of the macroscopic plastic flow. Further, shape of the curve is consistent with the step function approximation used in eq. (6.2) for determining the material parameters. The initial hardening rate term, $\dot{Z}_0$ in eq. (6.11) is responsible for characterizing the initial microstructure and influences the subsequent inelastic response. The transistion, from one term to the other, depends on strain rate and produces the various responses in calculated curves. This effect arose as a direct result of the potential function formulation.

If the initial hardness, Z_0, is lowered to near zero, the response becomes unstable between cycles of strain hardening and recovery as shown in fig. 4a. This effect has been observed in chemical lead at 29°C by Morrow and Halford (ref. 22) as shown in fig. 4b). They documented the effect as cyclic hardening and recovery. The calculated response in fig. 4a underscores the importance of the Z_0 and $\dot{Z}_0$ terms.

The predicted and observed response to a hysteresis loop with a 25 second hold in compression is shown in fig. 5. The overall dimensions on the observed and predicted response are close including the compressive stress relaxation response. The shape of the predicted curve near yield on loading in compression and reloading in tension reflects the assumption of isotropic hardening. Obviously, there is a small element of kinematic hardening being observed in the response.

Next, let us investigate the effect of initial load history on the subsequent creep response. This was done for the four initial strain rate histories and one creep stress as shown in fig. 6a. The predicted response curves have a very pronounced variation. Increasing the initial strain rate from 1.33×10^{-1} Sec^{-1} to 8.33×10^{-4} in four steps produces increases in creep strain rate.

The observed creep response for IN100 for six levels of creep stress is shown in fig. 6b. It was expected that increasing stress would produce creep curves ordered with increasing creep rates. However, creep curve 20 is not ordered with respect to the other curves. If the increase creep stress of 21 MPa between curves 19 and 20 is accompanied by a decrease in the initial strain rate, the observed response could be predicted.

Further evidence of the effect of initial strain rate on the subsequent response is shown in fig. 7 for Rene´ 95 at 649°C. All four tests were run using the creep stress of 1034.3 MPa. Two tests were run on a creep frame with the weights placed, one at a time, on a load pan. This produced a "slow" initial strain rate. The other two tests were run in a hydraulic closed loop testing system with the initial load applied rather rapidly producing a "fast" initial strain rate. There is significant variation in the observed creep response that might be attributed to the variation in initial strain rate. However, the two sets of tests were run in different laboratories on different heats of the material.

The effect of initial strain rate on stress relaxation was also investigated. Shown in Fig. 8 are four stress relaxation curves that were calculated using four different initial strain rates to a strain of 0.01. The initial strain rate has a dramatic influence on the initial stress as might be expected from the tensile curves. The initial rate of stress relaxation and the final stress level both appear to depend on the initial strain rate. The observed stress relaxation from 0.01 strain is also shown. This curve is part of a creep and recovery history with a subsequent deformation to 0.01 strain.

VIII SUMMARY

The potential function formulation for the state variable evolution equation was based on a combined inequality that allowed for both strain hardening and recovery. The resulting evolution law demonstrated both of these properties. In particular the derived evolution equation required initial values for both the state variable, Z, and its rate, $\dot{Z}$. In a given heat of material, with a fixed initial microstructure, the corresponding initial value for the state variable, Z, is assumed constant for all tests. However, the initial hardening rate, $\dot{Z}$, depends on how the specimen is initially loaded. This permits the equation to account for the formation of different initial microstructures with different properties that can effect the subsequent macroscopic inelastic flow.

This effect was investigated and the results can produce response curves that are not similar or even ordered under various loading conditions. These effects were observed in IN100, Rene' 95 and chemical lead at high temperature. Thus, it is possible that the variations in the initial loading condition could account for atleast some of the variations observed high temperature tests. This could be particularly useful for explaining the large amount of scatter observed in creep tests.

REFERENCES

1. Hill R., Mathematical Theory of Plasticity, Oxford University Press, 1950, Chapter III.

2. Drucker D.C., "Plasticity," Structural Mechanics (Proceedings First Symposium on Naval Structural Mechanics), Goodier J.H. and Hoff N.J., ed., Pergamon Press, 1960, p. 407.

3. Reed-Hill R.E., Physical Metallurgy Principles,, Van Nostrand, 1973.

4. Narayana A.D., "A Representation for the Deformation of a Metal Including the Effects of Strain Hardening and Recrystallization." Ph.D. Dissertation, University of Cincinnati, 1979.

5. Moteff J., "Deformation Induced Microstructural Changes in Metals," Proceedings Workshop on a Continuum Mechanics Approach to Damage and Life Prediction, Stouffer D.C., Krempl E. and Fitzgerald E.J., ed., Carrollton Kentucky, 1980, p. 11.

6. Ponter A.R.S., "Dynamic Behavior of Structures Composed of Strain and Work Hardening Visco-Plastic Materials," Journal of Solids and Structures, V 16, 1980, p. 793.

7. Rice J.R., "On the Structure of Stress Strain Relations for Time-Dependent Plastic Deformation of Metals," Journal Applied Mechanics, V37, pp 728-737, 1970.

8. Ponter A.R.S. and F.A. Leckie, "Constitutive Relationships for the Time Dependent Deformation of Metals," Journal of Engineering Materials and Technology," V98, pp 47-51, 1976.

9. Bailey R.W., "Note on the Softening of Strain Hardening Metals and its Relation to Creep," Journal of the Institute of Metals, V 35, pp 27-40, 1926.

10. Orowan E., "The Creep of Metals," J. West Scot Iron and Steel Institute, V 54, pp 45-53, 1946.

11. Bodner S.R. and Partom Y., "A Large Deformation Elastic-Viscoplastic Analysis of Thick-Walled Spherical Shell," Journal Applied Mechanics, V 39, pp 751-757, 1972.

12. Bodner S.R. and Partom Y., "Constitutive Equations for Elastic Viscoplastic Strain Hardening Materials," Journal Applied Mechanics, V 42, pp 385-389, 1975.

13. Stouffer D.C. and Bodner S.R., "A Relationship Between Theory and Experiment for a State Variable Constitutive Equation" ASTM-STP 765, Mechanical Testing and Deformation Model Development, 1982.

14. Stouffer D.C., "A Constitutive Representation for IN100," AFWAL-TR-81-4039, Wright Patterson AFB Ohio.

15. Gilman J.J., Micromechanics of Flow, McGraw-Hill New York, 1969.

16. Vreeland T.J., "Dislocation Velocity Measurements," Techniques of Metals Research, 2.1, Bunshak R.F. ed., Interscience Publ. p. 341, 1968.

17. Ponter A.R.S., Convexity and Associated Continuum Properties of a Class of Constitutive Relationship, Journal De Mécanique, 5.4, pp 527-541, 1976.

18. Merzer A. and Bodner S.R., ASME Journal of Engineering Materials and Technology, Vol. 101, 1979, pp 254-257.

19. Stouffer D.C. and Bodner S.R., "A Constitutive Equation for Deformation Induced Anisotropic Behavior of Metals," Intern. Journ. Engrg. Science, 17, 1979, p. 737.

20. Bodner S.R. and Stouffer D.C., "Comments on Anisotropic Plastic Flow and Incompressibility" to appear. Intern. Journ. Engrg. Science, 1982.

21. Stouffer D.C., Papernik L., and Bernstein H.L., "An Experimental Evaluation of the Mechanical Response Characteristics of Rene´ 95." Technical Report AFWAL-TR-80-4136, Air Force Wright Aeronautical Laboratory, Dayton, Ohio, 1980.

22. Morrow J. and Halford G.R., "Creep under Repeated Stress Reversals," Joint International Conference on Creep, New York, 1969, pp 343-47.

TABLE 1. SUMMARY OF THE EXPERIMENTAL PROGRAM

| Test No.	Type of Test	Spec. No.	Control Variable	Observed Variable	Comments
2	Tensile	G1	$\dot{\epsilon} = 1.42 \times 10^{-3} s^{-1}$	$\sigma = 1116$ MPa	
3	Tensile	T1	$\dot{X} = 8.33 \times 10^{-4} s^{-1}$		Const. Hd. Rate
4	Tensile	T3	$\dot{\epsilon} = 8.33 \times 10^{-4} s^{-1}$	$\sigma = 1068$ MPa	
5	Tensile	G2	$\dot{\epsilon} = 6.33 \times 10^{-5} s^{-1}$	$\sigma = 951$ MPa	
6	Tensile	ENTEN 1	$\dot{\epsilon} = 5.5 \times 10^{-5} s^{-1}$	$\sigma = 978$ MPa	
7	Tensile	GT7	$\dot{\epsilon} = 1.33 \times 10^{-5} s^{-1}$	$\sigma = 889$ MPa	
8	Tensile	ENTEN 4	$\dot{\epsilon} = 6.67 \times 10^{-6} s^{-1}$	$\sigma = 841$ MPa	
9	Tensile	G3	$\dot{\epsilon} = 1.67 \times 10^{-6} s^{-1}$		
10	Creep	C1	$\sigma = 496$ MPa	$\dot{\epsilon} = 1.8 \times 10^{-8} s^{-1}$	
14	Creep	GT6	$\sigma = 627$ MPa	$\dot{\epsilon} = 5.0 \times 10^{-8} s^{-1}$	
15	Creep	GT5	$\sigma = 620$ MPa	$\dot{\epsilon} = 1.2 \times 10^{-7} s^{-1}$	
16	Creep	C4	$\sigma = 696$ MPa		Relax. Obs
18	Creep	GT4	$\sigma = 827$ MPa	$\dot{\epsilon} = 4.5 \times 10^{-6} s^{-1}$	
19	Creep	C5	$\sigma = 875$ MPa	$\dot{\epsilon} = 7.74 \times 10^{-6} s^{-1}$	
20	Creep	ENTEN 2	$\sigma = 896$ MPa	$\dot{\epsilon} = 4.17 \times 10^{-6} s^{-1}$	
21	Combined History	C3	$\dot{\epsilon} = 4.0 \times 10^{-3} s^{-1}$		Hyst. Loop
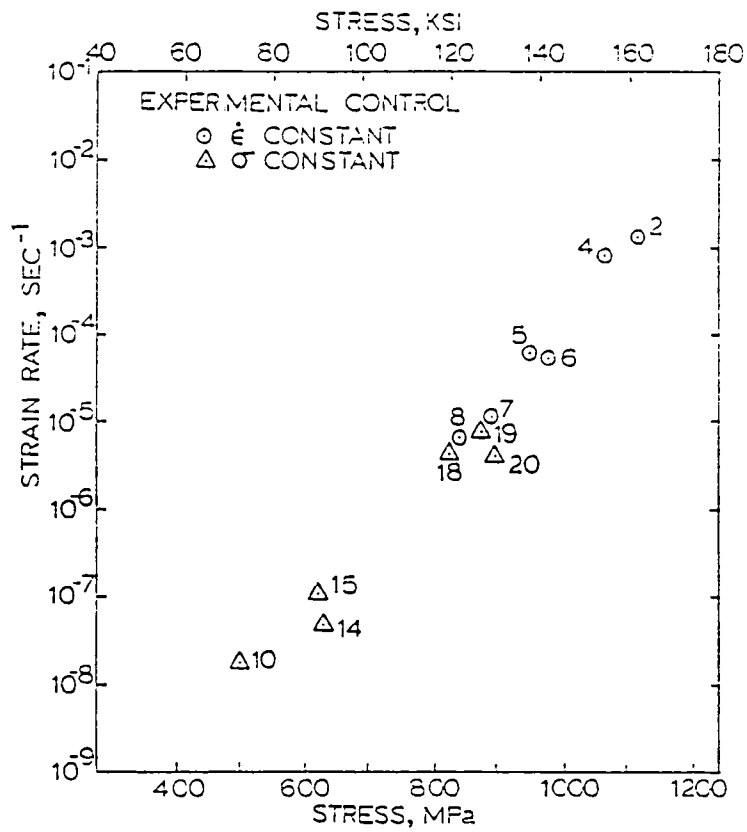
Figure 1. Stable values of stress and strain rate from both tensile and creep experiments. Test number refer to table 1.
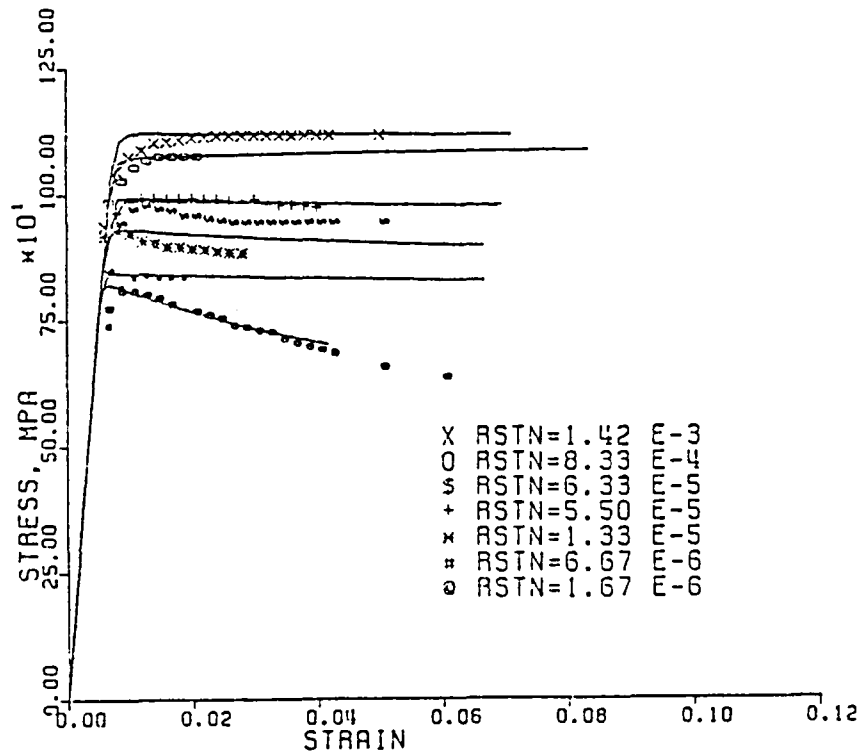
Figure 2. Calculated and observed tensile response curves for IN100 at 732°C for several constant strain rate load histories.
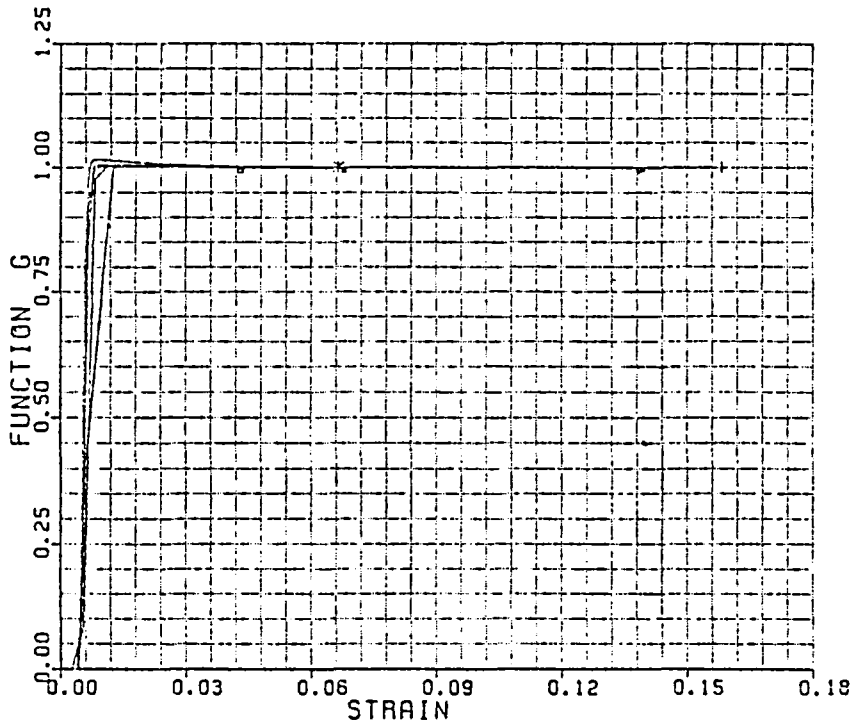

Figure 3. Response function $G = [(I(0) - I(R)] / [I(0) - I(\dot{\varepsilon}_0)]$ for the tensile response histories shown in figure 1.
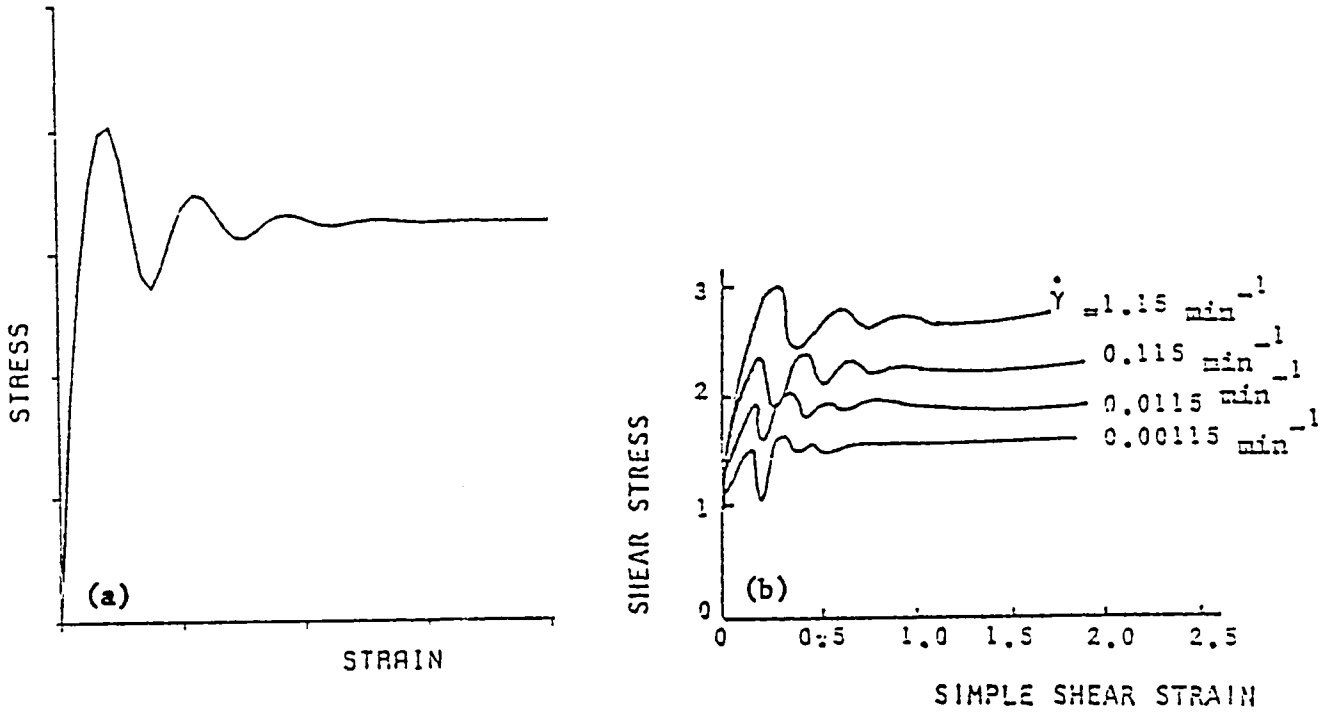
Figure 4. (a) Tensile responses characteristics of the model for an initial hardness near zero.

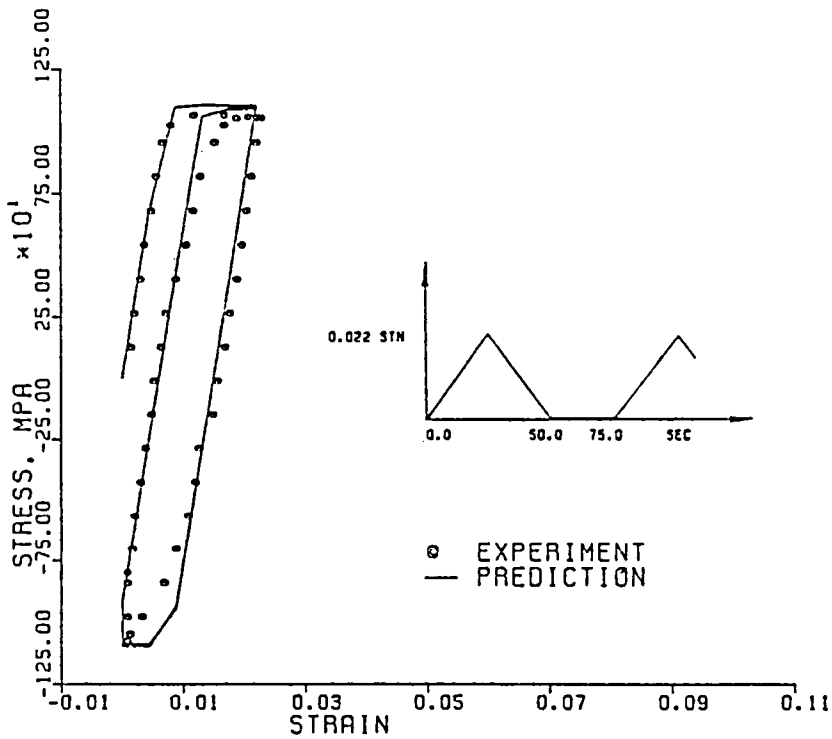(b) Observed tensile response for chemical lead at 29°C in simple shear. (After Morrow and Halford [22]).

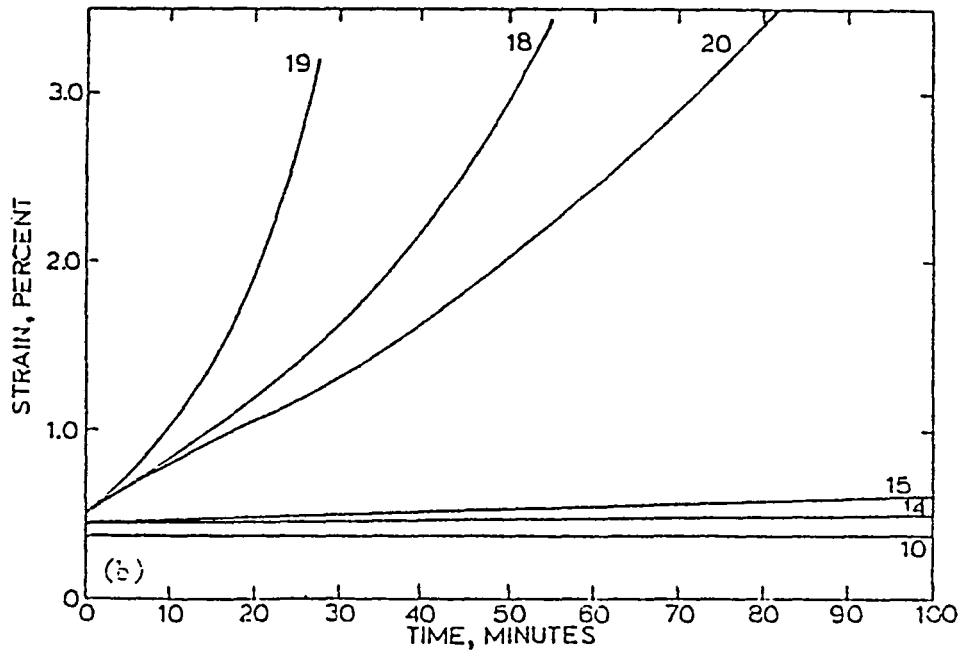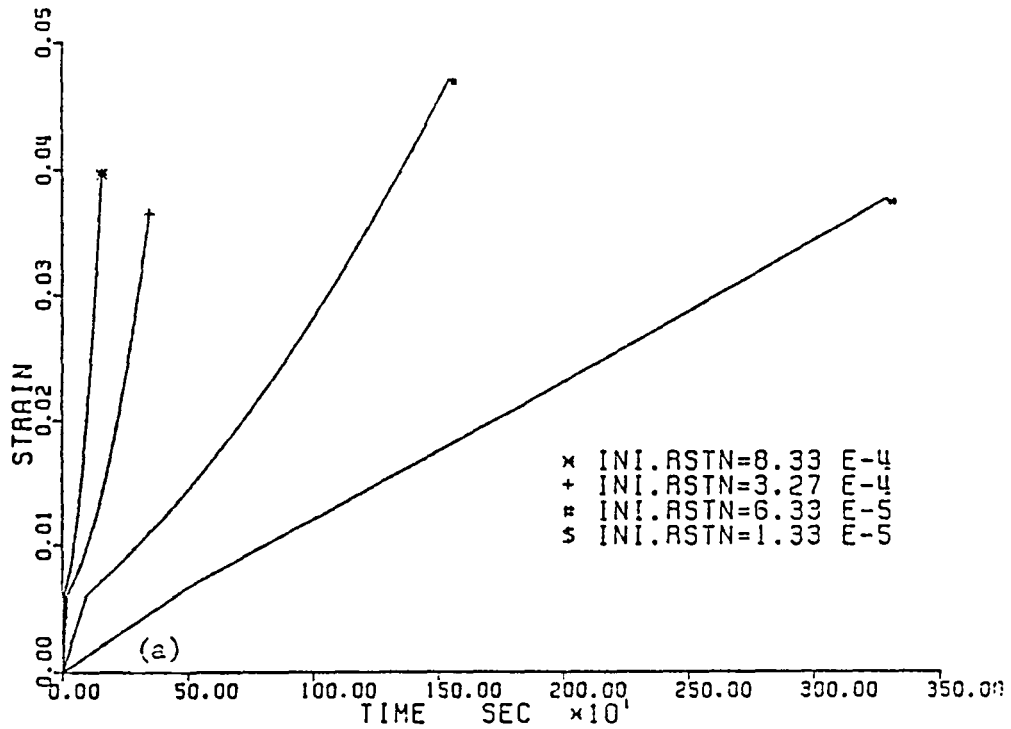Figure 5. Predicted and observed hysteresis loop response of IN100 at 732°C.

STRAIN

0.05 0.04 0.03 0.02 0.01 0.00

× INI.RSTN=8.33 E-4
+ INI.RSTN=3.27 E-4
# INI.RSTN=6.33 E-5
S INI.RSTN=1.33 E-5

(a)

0.00   50.00   100.00   150.00   200.00   250.00   300.00   350.00

TIME   SEC   ×10¹

STRAIN, PERCENT

3.0

2.0

1.0

0

19

18

20

15
14

10

(b)

0   10   20   30   40   50   60   70   80   90   100

TIME, MINUTES

Figure 6. (a) Predicted tensile creep response of IN100 at 732°C for a
                Creep stress of 896 MPa and several different initial load
                rates.

           (b) Observed tensile creep response of IN100 at 732°C for several
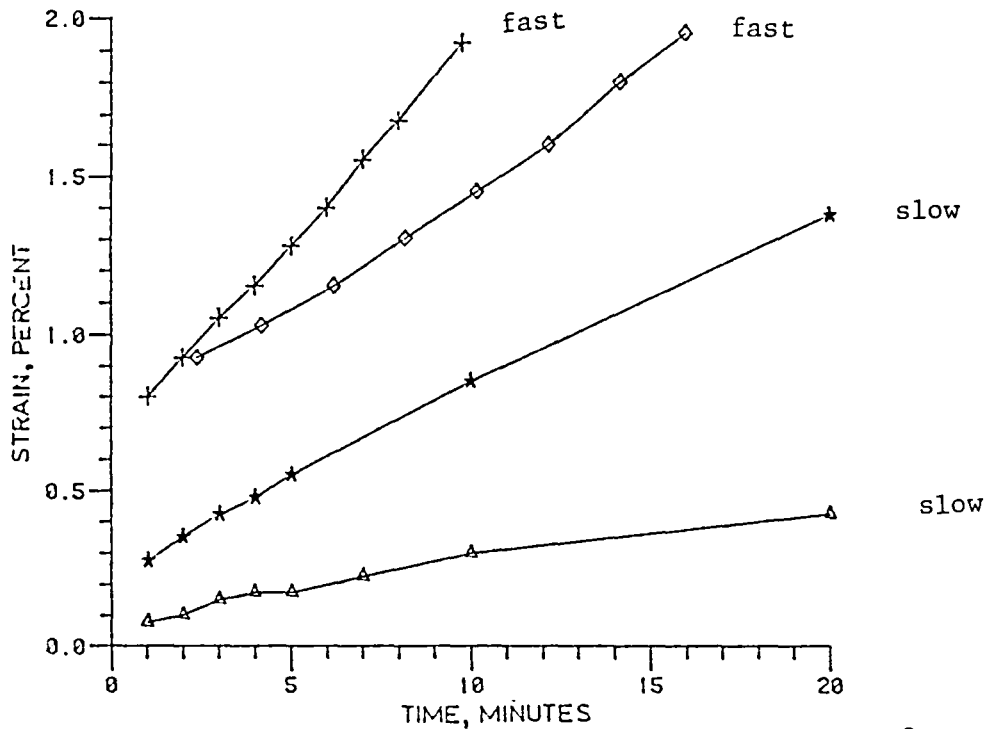   different stress histories with random initial load rates.

176

Figure 7. Observed tensile creep response of Rene´ 95 at 649°C at 1034.3 MPa with "fast" and "slow" initial load rates.
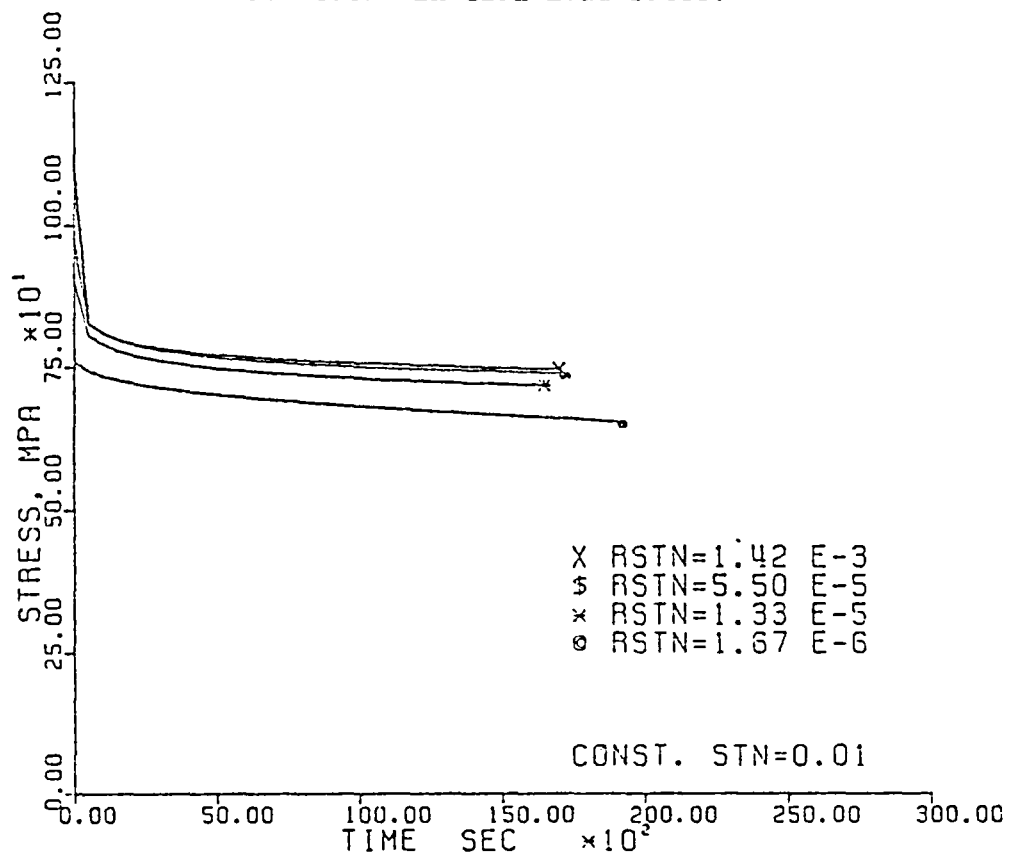

Figure 8. Predicted and observed stress relaxation responses of IN100 at 732°C at 0.01 strain with several initial load rates. Observed response at the same strain but with an unknown initial load history.